Appl. Phys. B (2017) 123:150
DOI 10.1007/s00340-017-6727-6

Applied Physics B
Lasers and Optics

Polarization contrast scattering spectroscopy of individual metal nanoantennas

Torsten Stiehm[1] · Johannes Kern[1] · Robert Schmidt[1] · Steffen Michaelis de Vasconcellos[1] · Rudolf Bratschitsch[1]

Received: 20 October 2016 / Accepted: 6 April 2017 / Published online: 19 April 2017

Abstract Metal nanoantennas give rise to strongly localized and enhanced electric fields. The enhancement is largest at the plasmon resonance, which, therefore, needs to be characterized. Here, we use polarization contrast microscopy for imaging and spectroscopy of single metal nanoantennas. The method relies on the strong suppression of incident linearly polarized light with a cross-polarized analyzer in the detection path and exploits the distinct polarization dependence of the plasmonic response of the antennas. The technique enables an easy-to-use background-free measurement of plasmon resonances of single metal nanoantennas in the visible and infrared spectral range.

1 Introduction

Optical nanoantennas [1] efficiently concentrate light in an area much smaller than the wavelength [2, 3]. Consequently, they play an important role in microscopy with sub-wavelength resolution [4]. The field localization is accompanied by an enhancement of the electric field, which can drastically boost linear and non-linear light–matter interactions. For example, strong enhancement has been observed for fluorescence [5, 6], surface-enhanced Raman scattering [7, 8], as well as for nonlinear light generation [9–12]. The reason for the strong field enhancement is the excitation of a resonant surface charge oscillation in the nanoantenna, i.e. the plasmon resonance. The frequency of the plasmon resonance depends strongly on the geometry, the material, and the dielectric environment of the nanoantenna [1, 13]. Therefore, it is indispensable to measure the plasmon resonance when coupling it to fundamental resonances in nanoemitters of light, such as single molecules, color centers in diamond, semiconductor quantum dots, or atomically thin semiconductors [14–16].

In recent years, a variety of methods have been developed to determine the plasmon resonances of single metal nanoantennas: darkfield scattering spectroscopy [17–19], photothermal imaging [20], cathodoluminescence [21], as well as polarization modulation spectroscopy [22–25]. However, the determination of the plasmon resonance of individual metal nanoantennas has proven to be difficult in the infrared (IR) spectral range at wavelengths above 1000 nm. Detectors based on InGaAs have to be used, which are noisy compared to silicon detectors. For this reason, spatial modulation techniques have been employed to boost the signal-to-noise ratio and measure the extinction spectrum of single metal nanostructures with resonances above 1000 nm [26–28]. Here, we present a simple approach to measure the plasmon resonances of single metal nanoantennas in the infrared as well as the visible spectral range. Our method is based on polarization microscopy [29–32] and exploits the suppression of incident linearly polarized light by a crossed analyzer in the detection path. We use the fact that a dipole nanoantenna exhibits a linear polarization and causes a positive polarization contrast signal with respect to the suppressed background. Since the background suppression relies entirely on polarization, the excitation and detection angles may be freely chosen, including normal incident light as well as large numerical apertures (NA >1.2). This is in contrast

Electronic supplementary material The online version of this article (doi:10.1007/s00340-017-6727-6) contains supplementary material, which is available to authorized users.

✉ Rudolf Bratschitsch
Rudolf.Bratschitsch@uni-muenster.de

[1] Institute of Physics and Center for Nanotechnology, University of Münster, 48149 Münster, Germany

to darkfield microscopy, which avoids the detection of the directly transmitted light by using different excitation and collection angles, e.g. excitation under high angles using a darkfield condenser and collection of the emission only under low angles. Polarization scattering spectroscopy can be easily integrated into existing transmission microscopes. The sample as well as all optical elements are not moved during the measurements, rendering the method very stable and easy to use. Consequently, polarization contrast scattering spectroscopy is expected to become a widely used tool for the in situ optical characterization of single metal nanoantennas.

2 Sample fabrication and polarization contrast scattering imaging

To demonstrate the method, we investigate nanoantennas consisting of two 30 nm high gold rods separated by a gap of 25 nm. The gold dimer nanoantennas are fabricated by electron-beam lithography and lift-off on a 170 µm fused silica substrate using a 2 nm chrome adhesion layer. Their widths (30–80 nm) and lengths (195–245 nm) are chosen such that the antennas have a plasmon resonance in the near-infrared spectral range between 1200 and 1400 nm.

We use a femtosecond Er:fiber laser (center wavelength 1.55 mm), which is spectrally broadened in a highly nonlinear fiber as a broadband infrared white light source [33]. The linear polarization of the laser is controlled by a polarizer to be either 0° or 45° with respect to the long axis of single gold dimer nanoantennas, as shown in Fig. 1a, c. For imaging, the light is focused on a single nanoantenna by an objective lens with a numerical aperture of NA = 0.9. The light is collected in transmission confocally through the substrate by an oil immersion objective lens (NA = 1.45) and detected by an InGaAs avalanche photodiode (Thorlabs APD130C). To record an image, the sample with the nanoantennas is scanned below the stationary laser focus. Figure 1b shows a confocal infrared transmission image of a 5 by 5 array of gold dimer nanoantennas. The antennas are visible as dark spots on a bright background. At the antenna positions a fraction of the incident light is absorbed and scattered away from the detector, whereas in the surroundings of the antennas the incident light passes through unchanged.

For polarization contrast scattering spectroscopy a polarizer acting as an analyzer is added behind the sample as depicted in Fig. 1c. The analyzer is oriented perpendicular to the polarization of the incident light and −45° with respect to the long axis of the nanoantenna. In that way, the polarization contrast signal is maximized and the incident light is suppressed by several orders of magnitude. If the orientation of the antenna is not known a priori, it can be found by maximizing the polarization contrast. In our experiment we measure a suppression by a factor of ~1300. Due to the plasmon resonance the light scattered by the nanoantenna is mainly polarized along the long axis of the antenna. Therefore, it partly passes the analyzer, which leads to bright spots at the position of the individual antennas (Fig. 1d). For the brightest antennas in Fig. 1d, this technique provides a contrast of 0.77, which is an enhancement of 6 compared to the transmission geometry (Fig. 1b).

3 Theoretical description

In this section the signal obtained in polarization contrast scattering microscopy is analytically described using the electric and magnetic fields. In particular it will be shown that the polarization contrast signal only depends on the scattering and not on the absorption of the nanoantenna.

In the absence of additional scatterers the total electric field $\boldsymbol{E}$ in the media surrounding the antenna is given by $\boldsymbol{E} = \boldsymbol{E}_\mathrm{i} + \boldsymbol{E}_\mathrm{scat}$, i.e. the sum of the incident field $\boldsymbol{E}_\mathrm{i}$ and the scattered field $\boldsymbol{E}_\mathrm{scat}$. A similar expression holds for the magnetic field: $\boldsymbol{H} = \boldsymbol{H}_\mathrm{i} + \boldsymbol{H}_\mathrm{scat}$. Both $\boldsymbol{E}$ and $\boldsymbol{H}$ are time- and space-dependent. Interference between the incident and scattered field leads to extinction, which is the sum of all losses due to scattering and absorption. The nanoantenna is oriented along the x-direction and the incident light is linearly polarized with an angle of 45° with respect to the long antenna axis. Assuming an antenna that radiates light, which is entirely polarized along the long antenna axis, the interaction between the antenna and the incident light only affects the electric (magnetic) field components parallel (perpendicular) to the long antenna axis. The other component remains unchanged. In this case the x- and y-components of the total electric and magnetic field can by approximated as follows:

$$\boldsymbol{E} = \boldsymbol{E}_\mathrm{i} + \boldsymbol{E}_\mathrm{scat} = \begin{pmatrix} \sqrt{E_\mathrm{i}} \\ \sqrt{E_\mathrm{i}} \end{pmatrix} + \begin{pmatrix} E_\mathrm{scat} \\ 0 \end{pmatrix};$$

$$\boldsymbol{H} = \boldsymbol{H}_\mathrm{i} + \boldsymbol{H}_\mathrm{scat} = \begin{pmatrix} -\sqrt{H_\mathrm{i}} \\ \sqrt{H_\mathrm{i}} \end{pmatrix} + \begin{pmatrix} 0 \\ H_\mathrm{scat} \end{pmatrix}.$$

The analyzer perpendicular to the polarization of the incident light in the detection path leads to the following expressions for the fields behind the analyzer in the Jones' matrix formalism:

$$\boldsymbol{E}_\mathrm{PC} = \tfrac{1}{2}\begin{pmatrix} 1 & -1 \\ -1 & 1 \end{pmatrix} \cdot \begin{pmatrix} \sqrt{E_\mathrm{i}} + E_\mathrm{scat} \\ \sqrt{E_\mathrm{i}} \end{pmatrix} = \tfrac{1}{2}\begin{pmatrix} E_\mathrm{scat} \\ -E_\mathrm{scat} \end{pmatrix} \text{ and}$$

$$\boldsymbol{H}_\mathrm{PC} = \tfrac{1}{2}\begin{pmatrix} 1 & 1 \\ 1 & 1 \end{pmatrix} \cdot \begin{pmatrix} -\sqrt{H_\mathrm{i}} \\ \sqrt{H_\mathrm{i}} + H_\mathrm{scat} \end{pmatrix} = \tfrac{1}{2}\begin{pmatrix} H_\mathrm{scat} \\ H_\mathrm{scat} \end{pmatrix}$$

The electric and magnetic fields are used to calculate the time-averaged Poynting vector $\boldsymbol{S}$. The power measured

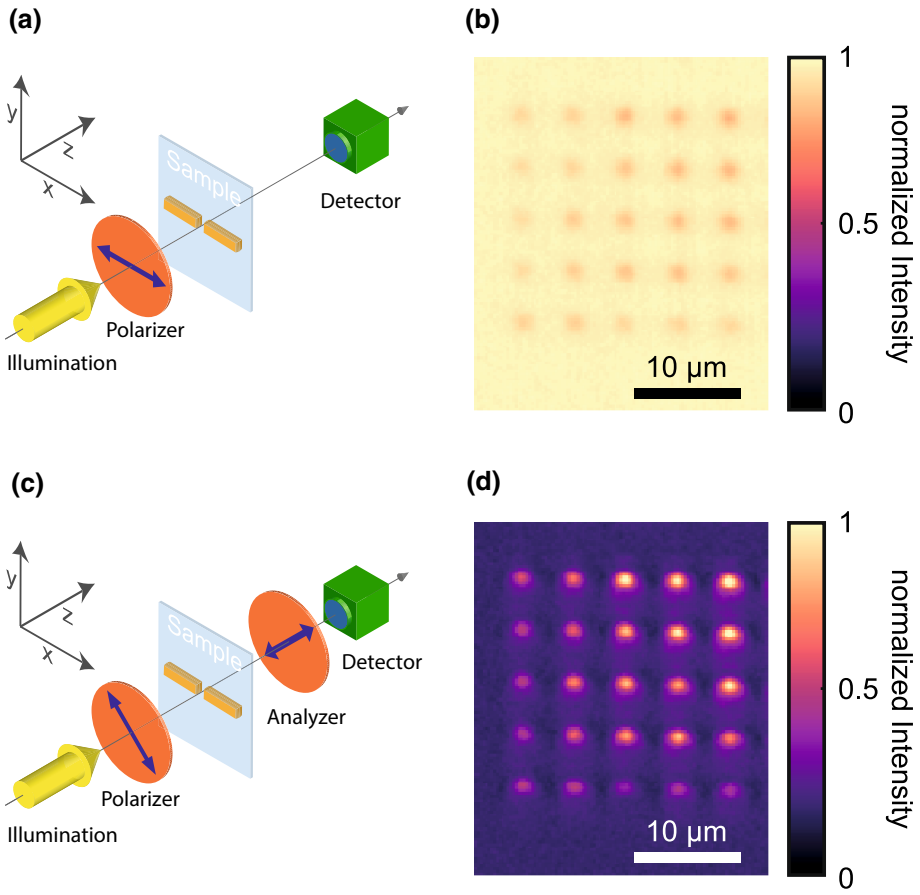

Fig. 1 Transmission microscopy and polarization contrast scattering microscopy. **a** Schematic drawing of the transmission geometry. **b** White light microscopy image in transmission geometry. The image exhibits a bright background. Gold dimer antennas appear as dark spots, because part of the incident light is scattered or absorbed by the antenna. The antennas are 200–240 nm long (increasing from *left* to *right*) and have a width of 30–80 nm (increasing from *top* to *bottom*). The gap between the antenna arms is 20 nm. **c** Schematic drawing of the polarization contrast scattering geometry. An additional polarizer (analyzer) is placed behind the sample at an angle of 90° with respect to the first polarizer and 45° with respect to the long axis of the nanoantenna. **d** Microscopy image in polarization contrast scattering geometry. The light used for excitation is blocked by the analyzer in the detection path, which is oriented perpendicular to the polarizer. This leads to a dark background around the antenna. The enhanced directional scattering due to the plasmon resonance of the individual nanoantennas causes a bright signal at the antenna positions

by a detector P_D in the *xy*-plane is given by the flux of the *z*-component of $\boldsymbol{S}$ through the detector area D.

In the absence of the analyzer (transmission geometry) the total power P_D consists of three components [34–36]: the incident power P_0, the power extinct by the antenna P_{ext}, and the power of the light scattered towards the detector $P_{s,D}$: $P_D = P_0 - P_{ext} + P_{s,D}$ (see A1 in the supporting information for complete derivation). In polarization contrast scattering geometry the detected power reduces to $P_{D,PC} = 1/2 \cdot P_{s,D}$ (see A1 for the complete derivation) and therefore, only the scattered light is detected. This is due to the analyzer, which removes the incident light. Thus, extinction, which is caused by interferences between incident and scattered light, will not be detected in this case.

This theoretical description can now be extended to calculate the spectra of a single dimer nanoantenna in transmission geometry and the polarization contrast scattering geometry. The frequency-dependent total electric and magnetic fields $\boldsymbol{E}$ and $\boldsymbol{H}$ are obtained numerically with a finite-difference time-domain algorithm (FDTD). The FDTD simulation setup mimics the experimental setup and is depicted in Fig. 2a. A gold dimer nanoantenna on a glass substrate has its long axis oriented along the *x*-direction at 0°. The antenna is excited from the air side by a focused Gaussian beam with linearly polarized light at an angle of 45°. A monitor large enough to collect all the incident light is placed inside the glass substrate directly behind the antenna. It detects $\boldsymbol{E}$ and $\boldsymbol{H}$, so that P_D can be calculated using the time-averaged Poynting vector $\boldsymbol{S}$. A simulation performed without antenna yields $\boldsymbol{E}_i$ and $\boldsymbol{H}_i$, so that one can compute $\boldsymbol{E}_{scat} = \boldsymbol{E} - \boldsymbol{E}_i$ as well as $\boldsymbol{H}_{scat}$. Figure 2 shows the detected power, normalized to the incident power

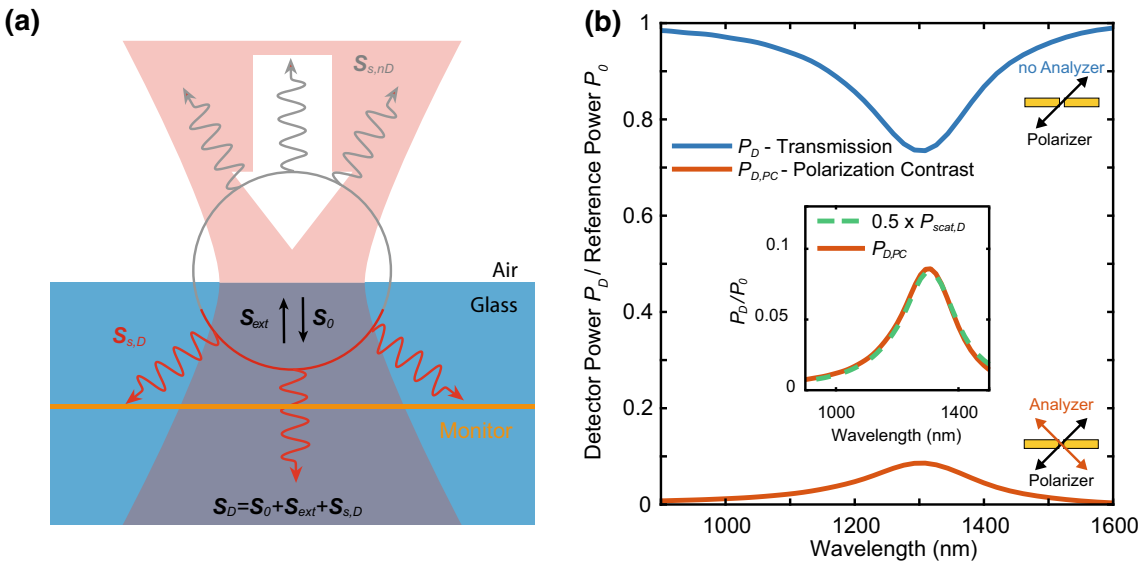

Fig. 2 Numerically calculated transmission and polarization contrast scattering spectroscopy signal of a single dimer nanoantenna. **a** Schematical drawing of the geometry used for the numerical simulation, indicating the direction of the incident light, the position of the monitor, and the components of the Poynting vector $\boldsymbol{S}_D$ responsible for the detected power. $\boldsymbol{S}_0$ and $\boldsymbol{S}_{s,D}$ are the Poynting vectors of the incident and the scattered light, respectively, whose interference leads to extinction $\boldsymbol{S}_{ext}$. $\boldsymbol{S}_{s,nD}$ is the scattered light, which does not reach the detector. **b** Calculated response of a gold dimer nanoantenna under linearly polarized white light illumination with and without an analyzer perpendicular to the excitation polarization and 45° with respect to the long antenna axis. The antenna arms have a length of 220 nm, a width of 38 nm and a height of 27 nm. The gap between the antenna arms is 30 nm. The power collected by a detector in transmission geometry (without the analyzer) is shown as a blue line. The power collected with polarization contrast (with the analyzer) is shown as a red line. The excitation geometries are sketched in the upper right und lower right corner, respectively. Inset: comparison between the detected power with an analyzer (*red solid line*) and half of the scattered power detected without an analyzer in the detection path (*green dashed line*)

P_0, without and with an analyzer perpendicular to the incident polarization, which represents the case of the transmission and the polarization contrast scattering geometry, respectively. Without the analyzer (transmission spectrum) the detected power is equal to the incident power diminished by the power absorbed by the nanoantenna and the power scattered in every but the direction of the monitor. This leads to a dip at the resonance frequency (Fig. 2b). Far away from the resonance no absorption or scattering occurs, yielding a signal of $P_D/P_0 = 1$.

The polarization contrast scattering spectrum is deduced from the detected electromagnetic field, by placing an analyzer at an angle of −45°, i.e. perpendicular to the incident field. Numerically, this is done using the Jones' matrices of the analyzer. A drastic change is observed in the spectrum. The polarization contrast scattering spectrum has a maximum at the resonance wavelength and vanishes far away from the resonance (Fig. 2b). We further compare the polarization contrast spectrum $P_{D,PC}$ and the scattered power collected $P_{s,D}$ (inset in Fig. 2b). This confirms the relation $P_{D,PC} = 1/2 \cdot P_{s,D}$, derived above. Small deviations occur because the excitation of the nanoantenna with a polarization angle of 45° results in a charge distribution which is not perfectly aligned along the long antenna axis. Nevertheless, the deviations are on the order of only 2%, justifying our assumption that the interaction between the antenna and the incident light mainly affects the electric (magnetic) field components parallel to the antenna.

4 Experimental results

In the experiment, polarization contrast scattering spectra are obtained by placing a monochromator in front of the detector. The detector signal is fed to a lock-in amplifier and the white light source is mechanically chopped with the lock-in reference frequency. The signal is normalized by dividing the cross-polarized transmitted intensity on the antenna I_{ant} by a co-polarized reference spectrum measured on the substrate I_{ref}. In that way, we are able to correct for the spectral shape of the light used for excitation. The measured spectra for three gold dimer nanoantennas with arm lengths of (197 ± 5), (205 ± 5) and (213 ± 5) nm, a width of (45 ± 5) nm and gaps of (25 ± 5) nm are shown in Fig. 3a. The spectra exhibit a Lorentzian shape with a full width at half maximum of 140 nm. As expected, the resonance shifts to the red from 1237 to 1368 nm as the antenna arm length is increased from (197 ± 5) to (234 ± 5) nm

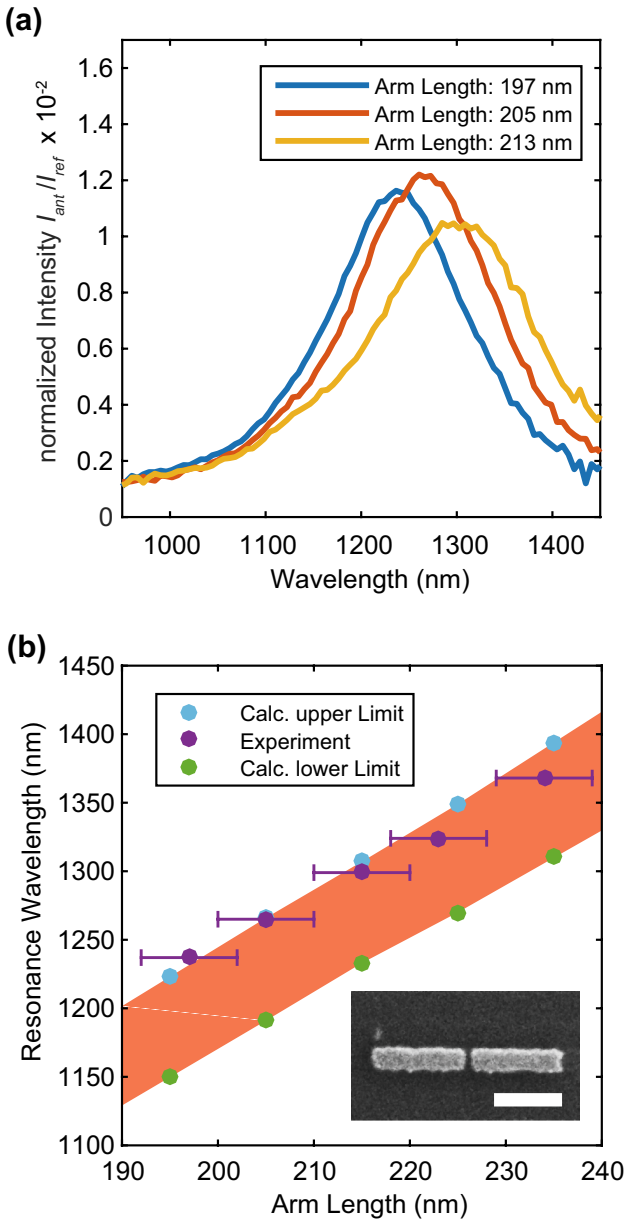

Fig. 3 **a** Measured polarization contrast scattering spectra of single gold dimer nanoantennas of 45 nm width, 25 nm gaps and different length, exhibiting resonances in the infrared. **b** Spectral positions of measured plasmon resonances of gold dimer nanoantennas with increasing arm length, a width of 45 nm, and gaps of 25 nm (*violet dots*). Also shown are the corresponding results extracted from calculated conventional scattering cross sections for a width of 40 nm and gap of 20 nm (*blue dots*), as well as for 50 nm wide antennas with a gap of 30 nm (*green dots*), i.e. the upper and lower limits in accordance with the experimental uncertainties in width and gap size (*red shaded area*). *Inset* Scanning electron microscope (SEM) image of a gold dimer nanoantenna. The *scale bar* corresponds to 200 nm

(Fig. 3b). We further numerically calculate conventional scattering cross sections for antennas of the same length using the FDTD algorithm and extract plasmon resonance wavelengths. The numerically obtained values are presented together with the experimental results in Fig. 3b. To account for uncertainties in the fabrication and determination of the antenna arm widths (45 ± 5 nm) and gap sizes (25 ± 5 nm) due to the polycrystalline nature of the gold nanoantennas (Fig. 3b), we perform several numerical calculations for this range. For a given antenna length the upper limit (blue dots) of the resonance wavelength is given by the antenna which has a small width (40 nm) and a small gap (20 nm), whereas the lower limit (green dots) of the resonance wavelength is given by the antenna which has a large width (50 nm) and a large gap (30 nm). As can be seen from Fig. 3b, there is an excellent agreement between calculation and experiment. Indeed, polarization contrast scattering spectroscopy can be used to determine the plasmon resonance of single metal nanoantennas.

We further demonstrate the validity of the new polarization contrast scattering technique by performing experiments in the visible regime. In this case, darkfield scattering spectroscopy can be performed and the plasmon resonances obtained by the two experimental techniques can be readily compared. As can be seen in Figure S1 (supporting information) we obtain a very good agreement between both techniques within measurement uncertainties of ±9 nm for both the spectral position and the full width at half maximum.

5 Conclusions

In conclusion, we have demonstrated polarization contrast scattering microscopy as an easy method to image nanoantennas with an enhanced contrast as compared to transmission microscopy. We successfully applied the technique to measure plasmon resonance spectra in the visible and infrared with a low background. We have compared the obtained results to darkfield scattering spectroscopy and FDTD simulations and found an excellent agreement. Polarization contrast scattering spectroscopy only requires two polarizers and does not rely on angular filtering or modulation techniques. Therefore, it can be easily integrated in existing experiments and provides a cheap, simple, and robust way for the in situ characterization of single plasmonic nanoantennas.

Acknowledgements We gratefully acknowledge financial support by the Deutsche Forschungsgemeinschaft (SPP 1391). We thank Harald Fuchs for granting access to the metal evaporator.

References

1. P. Biagioni, J.-S. Huang, B. Hecht, Rep. Prog. Phys. **75**, 024402 (2012)

2. J.A. Schuller, E.S. Barnard, W. Cai, Y.C. Jun, J.S. White, M.L. Brongersma, Nat. Mater. **9**, 193 (2010)
3. N. Liu, M.L. Tang, M. Hentschel, H. Giessen, A.P. Alivisatos, Nat. Mater. **10**, 631 (2011)
4. R. Zhang, Y. Zhang, Z.C. Dong, S. Jiang, C. Zhang, L.G. Chen, L. Zhang, Y. Liao, J. Aizpurua, Y. Luo, J.L. Yang, J.G. Hou, Nature **498**, 82 (2013)
5. S. Kühn, U. Håkanson, L. Rogobete, V. Sandoghdar, Phys. Rev. Lett. **97**, 017402 (2006)
6. A. Kinkhabwala, Z. Yu, S. Fan, Y. Avlasevich, K. Müllen, W.E. Moerner, Nat. Photon. **3**, 654 (2009)
7. S. Nie, S.R. Emory, Science **275**, 1102 (1997)
8. J.P. Camden, J.A. Dieringer, Y. Wang, D.J. Masiello, L.D. Marks, G.C. Schatz, R.P. Van Duyne, J. Am. Chem. Soc. **130**, 12616 (2008)
9. T. Hanke, G. Krauss, D. Träutlein, B. Wild, R. Bratschitsch, A. Leitenstorfer, Phys. Rev. Lett. **103**, 257404 (2009)
10. P. Biagioni, D. Brida, J.-S. Huang, J. Kern, L. Duò, B. Hecht, M. Finazzi, G. Cerullo, Nano Lett. **12**, 2941 (2012)
11. M. Sivis, M. Duwe, B. Abel, C. Ropers, Nat. Phys. **9**, 304 (2013)
12. T. Stiehm, J. Kern, M. Jürgensen, S.M. de Vasconcellos, R. Bratschitsch, Appl. Phys. B **122**, 1 (2016)
13. K.M. Mayer, J.H. Hafner, Chem. Rev. **111**, 3828 (2011)
14. V. Giannini, A.I. Fernández-Domínguez, S.C. Heck, S.A. Maier, Chem. Rev. **111**, 3888 (2011)
15. J. Wolters, G. Kewes, A.W. Schell, N. Nüsse, M. Schoengen, B. Löchel, T. Hanke, R. Bratschitsch, A. Leitenstorfer, T. Aichele, O. Benson, Phys. Status Solidi B **249**, 918 (2012)
16. J. Kern, A. Trügler, I. Niehues, J. Ewering, R. Schmidt, R. Schneider, S. Najmaei, A. George, J. Zhang, J. Lou, U. Hohenester, S. Michaelis de Vasconcellos, R. Bratschitsch, ACS Photon. **2**, 1260 (2015)
17. C. Sönnichsen, T. Franzl, T. Wilk, G. von Plessen, J. Feldmann, O. Wilson, P. Mulvaney, Phys. Rev. Lett. **88**, 077402 (2002)
18. O.L. Muskens, V. Giannini, J.A. Sánchez-Gil, J. Gómez, Rivas. Opt. Express **15**, 17736 (2007)
19. J.A. Fan, K. Bao, J.B. Lassiter, J. Bao, N.J. Halas, P. Nordlander, F. Capasso, Nano Lett. **12**, 2817 (2012)
20. S. Berciaud, D. Lasne, G.A. Blab, L. Cognet, B. Lounis, Phys. Rev. B **73**, 045424 (2006)
21. T. Coenen, E.J.R. Vesseur, A. Polman, ACS Nano **6**, 1742 (2012)
22. C. Sönnichsen, A.P. Alivisatos, Nano Lett. **5**, 301 (2005)
23. C.R. Carey, T. LeBel, D. Crisostomo, J. Giblin, M. Kuno, G.V. Hartland, J. Phys. Chem. C **114**, 16029 (2010)
24. G. Lilley, K. Unterrainer, Opt. Express **21**, 30903 (2013)
25. S. Chandel, J. Soni, S. kumar Ray, A. Das, A. Ghosh, S. Raj, N. Ghosh, Sci. Rep. **6**, 26466 (2016)
26. M. Husnik, M.W. Klein, N. Feth, M. König, J. Niegemann, K. Busch, S. Linden, M. Wegener, Nat. Photon. **2**, 614 (2008)
27. M. Husnik, S. Linden, R. Diehl, J. Niegemann, K. Busch, M. Wegener, Phys. Rev. Lett. **109**, 233902 (2012)
28. L.-J. Black, Y. Wang, C.H. de Groot, A. Arbouet, O.L. Muskens, ACS Nano **8**, 6390 (2014)
29. X. Hong, E.M.P.H. van Dijk, S.R. Hall, J.B. Götte, N.F. van Hulst, H. Gersen, Nano Lett. **11**, 541 (2011)
30. D.B. Murphy, M.W. Davidson, *Fundamentals of light microscopy and electronic imaging*, 2nd edn. (Wiley-Blackwell, Hoboken, 2012)
31. Y. Chen, X. Chen, Q. Cao, K. Xu, Plasmonics **10**, 1883 (2015)
32. X. Ding, F. Monticone, K. Zhang, L. Zhang, D. Gao, S.N. Burokur, A. de Lustrac, Q. Wu, C.-W. Qiu, A. Alù, Adv. Mater. **27**, 1195 (2015)
33. A. Sell, G. Krauss, R. Scheu, R. Huber, A. Leitenstorfer, Opt. Express **17**, 1070 (2009)
34. C.F. Bohren, D.R. Huffman, *Absorption and scattering of light by small particles* (Wiley-VCH, New York, 1998)
35. N.M. Mojarad, V. Sandoghdar, M. Agio, J. Opt. Soc. Am. B **25**, 651 (2008)
36. A. Crut, P. Maioli, N.D. Fatti, F. Vallée, Chem. Soc. Rev. **43**, 3921 (2014)